

Taming Large Multimodal Agents for Ultra-low Bitrate Semantically Disentangled Image Compression

Juan Song¹ Lijie Yang¹ Mingtao Feng^{2,*}

¹School of Computer Science and Technology, Xidian University

²School of Artificial Intelligence, Xidian University

songjuan@mail.xidian.edu.cn, 23031212033@stu.xidian.edu.cn, mintfeng@hnu.edu.cn *

Abstract

It remains a significant challenge to compress images at ultra-low bitrate while achieving both semantic consistency and high perceptual quality. We propose a novel image compression framework, Semantically Disentangled Image Compression (SEDIC) in this paper. Our proposed SEDIC leverages large multimodal models (LMMs) to disentangle the image into several essential semantic information, including an extremely compressed reference image, overall and object-level text descriptions, and the semantic masks. A multi-stage semantic decoder is designed to progressively restore the transmitted reference image object-by-object, ultimately producing high-quality and perceptually consistent reconstructions. In each decoding stage, a pre-trained controllable diffusion model is utilized to restore the object details on the reference image conditioned by the text descriptions and semantic masks. Experimental results demonstrate that SEDIC significantly outperforms state-of-the-art approaches, achieving superior perceptual quality and semantic consistency at ultra-low bitrates (≤ 0.05 bpp). Our code is available at <https://github.com/yang-xidian/SEDIC>.

1. Introduction

With the recent advancements in 5G [21] and 6G [49], the integration of numerous embedded devices and Internet-of-Things devices into communication protocols has posed challenges due to limited storage resources and extreme channel conditions. Ultra-low bitrate image compression research aims to address these challenges through compressing an image to one-thousandth of its original size or even smaller, thus dramatically reducing storage and bandwidth requirements. It remains a significant challenge to reconstruct images with satisfactory perception quality due to substantial information loss during compression.

*Corresponding author.

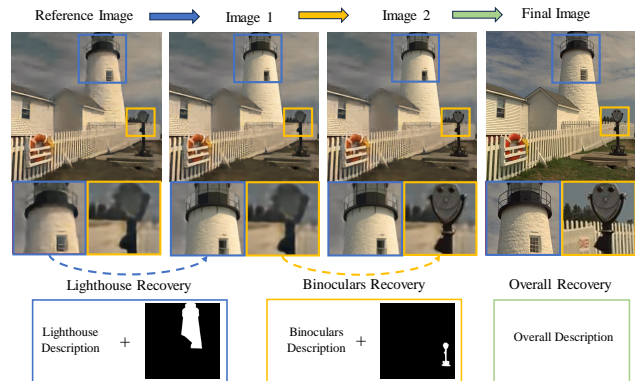


Figure 1. The proposed multi-stage semantic image decoding leverages controllable diffusion models to restore adequate details starting from the reference image object-by-object progressively conditioned by object descriptions and masks. Finally, the overall description are used to enhance the overall perceptual quality.

Traditional block-based compression codecs, e.g., JPEG [43], VVC [40], are constrained to use large quantization steps in such scenarios, inevitably leading to noticeable blurring and blocking artifacts. Despite the superior rate-distortion (R-D) performance of learning-based compression techniques [4, 5, 29, 31] that follow the Variational Autoencoders (VAEs), these methods produce blurry images at ultra-low bitrates, due to the reliance on optimization of pixel-oriented distortion metrics as measured by Peak Signal-to-Noise Ratio (PSNR) and Multi-Scale Structural Similarity Index Measure (MS-SSIM).

In order to achieve such extreme compression ratios, Generative Image Compression (GIC) shifts the focus from low-level fidelity to semantic consistency with the reference image. Early GIC implementations utilized Generative Adversarial Networks (GANs) as decoders, offering the potential for ultra-low bitrate compression. Afterwards, GAN is gradually replaced by Diffusion constrained with multimodal information such as text, edge. The rise of large multimodal models has further ushered in new paradigms for ultra-low bitrate image compression. Leveraging great

understanding capabilities of state-of-the-art Large Multimodal Models (LMMs), such as GPT-4 Vision [1], Llama [42], and the generative power of Stable Diffusion [39] and DALL-E [37], image data can be efficiently encoded into compact semantic representations, facilitating high-quality reconstructions even under extreme compression constraints. For instance, Lei et al. [19] directly transmit short text prompts and image sketches, employing the pre-trained ControlNet [46] to produce reconstructions with high perceptual quality. However, current text-to-image models such as Stable Diffusion [39] and DALL-E [37] still struggle to deal with complicated prompts involving content details, resulting in semantic detail inconsistency with the original image. That motivates us to think about the question: *How to extract adequate details and guide the image reconstruction leveraging the power of LMMs to maintain the trade-off between perception and consistency in ultra-low bitrate image compression?*

As we all know, the human perception of an image is usually progressive. Our eyes tend to first capture an overview of the image at a glance, which tends to be unfocused and blurred with low quality. Subsequently, by directly focusing on the objects of interest, our eyes can acquire detailed and high-resolution information regarding the objects. Inspired by this biological phenomenon, we design a novel SEMantically Disentangled Image Compression (SEDIC) framework to imitate this progressive perception. Initially, a low-quality reference image is obtained through a learned image encoder at ultra-low bitrate. Then we leverage LMMs to extract and encode essential semantic information regarding the objects of interest at the minimal bitrate cost, including image overall description, object detailed description and semantic segmentation masks. As illustrated in Figure 1, We design a multi-stage semantic image decoder that leverage pre-trained controllable text-to-image diffusion models to restore the low quality reference image with adequate details object-by-object progressively, conditioned by the text descriptions and semantic masks, ultimately generating high-quality reconstructions that are highly consistent with the original image. The contributions of this paper are summarized as follows.

- We propose a semantically disentangled image compression framework by leveraging the great comprehension capacity of LMMs to encode the image into compact semantic information at the object level to achieve ultra-low bitrate compression.
- We design a multi-stage semantic decoder which performs decoding object-by-object progressively starting from the low-quality reference image, ultimately generating high-quality and high-fidelity reconstructions. In each stage, pre-trained controllable diffusion model are used to restore details conditioned by the transmitted text descriptions and semantic segmentation masks.

- Both qualitative and quantitative results demonstrate that proposed SEDIC achieves a significant improvement compared to SOTA codecs in terms of perceptual quality metrics at ultra-low bitrates ($\leq 0.05\text{bpp}$).

2. Related Work

Ultra-low Bitrate Image Compression. Compression paradigm shifts the focus from low-level fidelity to semantic consistency with the original image to achieve ultra-low bitrate. Early image compression implementations [28, 32] utilized GANs as decoders, offering the potential for ultra-low bitrate compression. Afterwards, GAN is gradually replaced by Diffusion due to its great generative capacity. Yang et al. [44] replaced the decoder network with a conditional diffusion model. Some works began to leverage pretrained text-to-image diffusion models as prior knowledge to achieve realistic reconstructions at extremely low bitrates. Pan et al. [34] encode images into short text embeddings and then generate high-quality images with pretrained text-to-image diffusion models. Lei et al. [19] utilized the image understanding capabilities of CLIP [36] and great generation abilities of the Stable Diffusion to compress images into short text descriptions and sketches to achieve ultra-low bitrate compression. Despite these advantages, they still struggle to achieve trade-off between the consistency and perceptual quality at such low bitrates.

Large Multimodal Models. Large Multimodal Models (LMMs) have brought their robust reasoning and comprehension capabilities to multimodal tasks, achieving significant progress in various visual tasks such as visual question answering [1, 25, 45] and document reasoning [17, 27]. Among these, Multimodal Large Language Models (MLLMs) have demonstrated exceptional ability in conversing and generating detailed image descriptions based on visual inputs. Notably, GPT-4 Vision [1] is the most advanced MLLM model that can simultaneously process text and image inputs, enabling richer understanding and generation capabilities. Meanwhile, Multimodal Large Vision Models have also demonstrated significant potential values in the domains of image understanding. Grounding DINO [26] serves as an open-set object detector allowing it to detect arbitrary objects based on human-provided inputs such as category names or referential expressions. The Segment Anything Model (SAM) [18], a recent foundation model for segmentation, generates high-quality masks from diverse prompts, including points, rough boxes, or other cues. In this work, we aim to leverage these LMMs to extract and encode compact semantic information from images at the cost of minimum bitrates.

Controllable Image Generation. Diffusion models have attracting attentions due to its powerful generative capability. Text-to-image generation [14] is one of the most popular applications, which aims to generate the high-quality

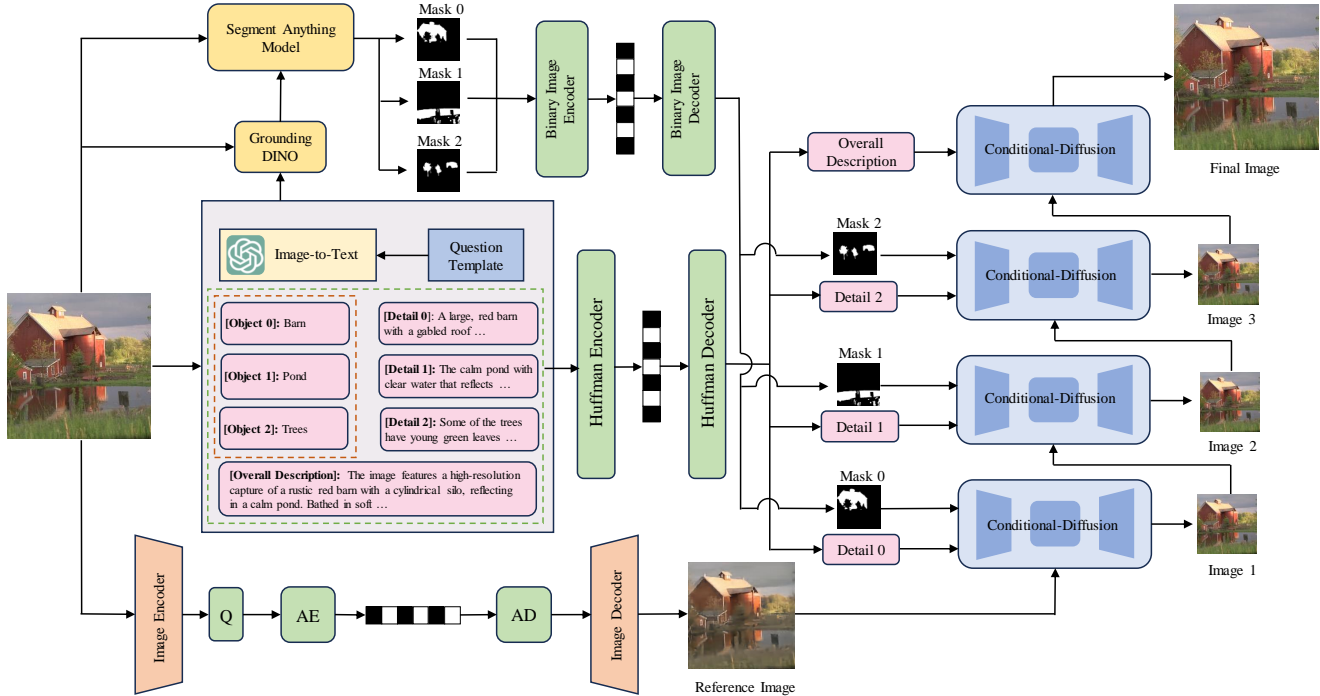


Figure 2. The SEDIC framework consists of a Semantically Disentangled Image Encoder and a Multi-stage Semantic Image Decoder. The Semantically Disentangled Image Encoder extracts overall and object detailed descriptions, semantic masks and the extremely compressed image. The Multi-stage Semantic Image Decoder progressively leverages the controllable diffusion models to progressively restore the details of the objects until the details of the entire image are restored conditioned by the aforementioned components.

image aligning with given text prompts. Additionally, several studies [3, 8, 47] further augmented controllability via add spatially localized input conditions, e.g., edges, depth, segmentation, human pose, etc., to a pretrained text-to-image diffusion model via efficient finetuning. Based on ControlNet[47], Lin et al.[24] proposed IRControlNet that leverages text-to-image diffusion prior for realistic image restoration. Li et al. [22] proposed a multimodal LLM agent (MuLan) that utilized a training-free multimodal-LLM agent to progressively generate objects with feedback control so that the whole generation process would be better controlled. We aim to exploit controllable image generation techniques for object-level semantic decoding, thereby maintaining high visual fidelity and perception quality.

3. Semantically Disentangled Image Compression Framework

In this section, we propose the Semantically Disentangled Image Compression framework, as illustrated in Figure 2. Specifically, the semantically disentangled image encoder is consisted of three encoding modules, including an image textualization encoder to extract overall and object-level detailed descriptions, a semantic mask encoder to annotate spatial information for each object, and an image encoder to obtain an extremely compressed reference image. The Multi-stage object-level semantic image decoder leverages

pre-trained conditional diffusion models to facilitate reconstruction object-by-object progressively starting from the extremely compressed image, conditioned by the decompressed text descriptions and semantic masks.

3.1. Semantically Disentangled Image Encoder

Image Textualization Encoder. Text description is the compact semantic representation of the image. Existing image compressors harnessing Image-to-Text models only used a brief and holistic text description lack of details to guide the generative decoders, which results in low fidelity with the ground truth although satisfying perception quality is achieved [19, 34]. Inspired by the work[35], we elaborately design an image textualization encoder to generate a comprehensive description of the entire image along with detailed descriptions of important objects. Specifically, it operates in two stages: fine-grained object textualization and coarse-grained holistic captioning. **Fine-grained Object Textualization.** We leverage the powerful visual understanding capabilities of the MLLM model to generate fine-grained object-level descriptions focusing on object attributes, such as shape, color, and texture, and etc. **Coarse-grained Holistic Captioning.** We further utilize the MLLM model to generate an overall description of the image with respect to the image resolution, content, style and etc. Despite lack of visual details, it includes the main

objects present in the image and the contextual information of the scene. Besides the object details, these elements are able to restore the texture details of the entire image to enhance the overall perception quality.

Specifically, to accurately extract object-level and overall text descriptions, we feed the prompts to the most advanced GPT-4 Vision [1] model for image textualization. The prompt template is illustrated in the supplementary material in detail. The following natural language feedback is obtained:

- $Textn_j$: Object Name ($\leq l_n$ words)
- $Textd_j$: Object Detail ($\leq l_d$ words)
- $Text_{all}$: Overall Image Description ($\leq l_{all}$ words)

Where $j \in \{0, 1, \dots, J - 1\}$, J represents the number of objects. It has been shown in [13] that as the number of descriptive terms increases, compression performance gradually improves, reaching a maximum at approximately 50 words. Therefore, we adjust l_{all} according to the compression level, with an upper limit of 50. **[Overall Image Description]** provides a holistic description of the image. **[Object Name]** is used as a prompt for semantic segmentation and is not transmitted to the decoder for reconstruction; its maximum word length l_n is set to 3. **[Object Details]** includes attributes such as object shape, color, condition, or other characteristics. Its word length l_d is dynamically adjusted based on the level of compression with an upper limit of 50. The greater the compression ratio, the smaller l_d , resulting in fewer details. Finally we utilize Huffman coding to losslessly compress the text information $\{Textn, Textd, Text_{all}\}$ at an ultra-low bitrate and transmit them to the decoder.

Even the most powerful MLLMs, such as GPT4-Vision, suffer from the hallucination issue. It may generate descriptions of objects that do not exist in the image. To prevent hallucinations and ensure that the generated object descriptions accurately correspond to the contents of the image, we utilize an open-set object detector (e.g., Grounding Dino [26]) to verify each of object in the descriptions are detected in the image. Any hallucinated object phrases, which are not found in the image, are tagged as "Hallucination" and removed from the text descriptions.

Semantic Mask Encoder. Since textual descriptions can only express relative left-right and above-below relationships in the image, they lack the ability to convey precise spatial relationship between objects needed in image reconstruction. To address this limitation, we propose a Semantic Mask Encoder that generates precise semantic segmentation masks given the object name $Textn$, to provide precise spatial information and edge contour for each object.

The SAM model [18] is an open-world segmentation model capable of isolating any object within an image when given appropriate prompts, such as points, boxes. However, SAM requires point or box prompts and does not directly

identify masked objects based on arbitrary text inputs. To address this issue, we combine the SAM model with an open-world object detector Grounding DINO [26] to support text inputs about the object. Grounding DINO is an open-world object detector with robust zero-shot detection capabilities that can detect bounding boxes by inputting object text. First, we input the object name into Grounding DINO to obtain the object’s bounding box, and then we pass the bounding box information to the SAM model to generate the semantic segmentation mask.

The semantic mask for each object, as a form of binary image, represents pixels in two distinct states—typically black and white, where each pixel is encoded using a single bit. Some binary image compression methods, e.g. JBIG2 [33], runlength coding [15], can be applied to further losslessly compress the semantic masks.

Image Encoder. The aforementioned text descriptions and semantic masks are obviously inadequate for the accurate decoding of the image. Such an approach would inevitably lead to a significant reduction in fidelity compared to the original image, akin to the findings in the related literature[19]. This is attributable to the substantial loss of critical information, such as structural details and color nuance, which are inherently challenging to encapsulate in natural language.

An extremely compressed representation of the original image can serve as a foundational reference of structural and color information for the generative decoder although this compressed representation captures only a severely degraded version of the original image and lacks texture details. When combined with the two aforementioned image textualization and semantic mask encoders, this extremely compressed image helps the subsequent generative decoder achieve satisfactory perceptual quality while maintaining consistency with the original image.

To obtain a reference image at an ultra-low bitrate, we retrained the existing deep learning-based image compression methods, such as the cheng2020-attn model in the deep image compression platform CompressAI [6]. Given an input image I , a pair of latent $y = g_a(I)$ and hyper-latent $z = h_a(y)$ is computed. The quantized hyper-latent $\hat{z} = Q(z)$ is modeled and entropycoded with a learned factorized prior. The latent y is modeled with a factorized Gaussian distribution $p(y|\hat{z}) = \mathcal{N}(\mu, \text{diag}(\sigma))$ whose parameter is given by the hyper-decoder $(\mu, \sigma) = h_s(\hat{z})$. The quantized version of the latent $\hat{y} = Q(y - \mu) + \mu$ is then entropy coded and passed through decoder g_s to derive reconstructed image $\tilde{I}_0 = g_s(\hat{y})$. The reconstructed image \tilde{I}_0 will serve as the starting point of the subsequent multi-stage semantic image decoding. The loss function \mathcal{L} of end-to-end training is formulated as,

$$\mathcal{L} = R(\hat{y}) + R(\hat{z}) + \lambda \cdot D(I, \tilde{I}_0) \quad (1)$$

where λ is the Lagrange multiplier regulating the trade-off

Algorithm 1 Multi-stage Semantic Image Decoding

Input: Reference image \tilde{I}_0 , text description $Text_{all}$, $Text_d$, semantic mask M , diffusion steps T , attention guidance timestep threshold T' , number of objects J , the CLIP text encoder, the fixed VAE encoder $\varepsilon(\bullet)$, the fixed VAE decoder $\mathcal{D}(\bullet)$, the pretrained ControlNet.

Output: Final Reconstructed Image \tilde{I}_F .

```
1: for  $j = 0 : J$  do
2:    $z_{j,T} \sim \mathcal{N}(0, \mathbf{I})$ 
3:    $cf_j = \varepsilon(I_j)$ ;
4:   if  $j < J$  then
5:      $ctd_j = CLIP(Text_d_j)$ ;
6:     for  $t = T : 0$  do
7:       if  $t > T'$  then
8:          $z_{j,t} = z_{j,t} - \eta \cdot \nabla_{z_{j,t}} E(A, M_j, k)$ ;
9:       end if
10:       $z_{j,t-1} = ControlNet(z_{j,t}, ctd_j, t, cf_j)$ ;
11:       $z_{j,(t-1)} = M_j \odot z_{j,t} + (1 - M_j) \odot z_{(j-1),(t-1)}$ ;
12:    end for
13:  else
14:     $ctd_j = CLIP(Text_{all})$ ;
15:    for  $t = T : 0$  do
16:       $z_{j,t-1} = ControlNet(z_{j,t}, ctd_j, t, cf_j)$ ;
17:    end for
18:  end if
19:   $\tilde{I}_{j+1} = \mathcal{D}(z_{j,0})$ ;
20: end for
21: return  $\tilde{I}_F = \tilde{I}_{J+1}$ 
```

between rate $R(\cdot)$ and distortion $D(\cdot)$. The larger the parameter λ , the large bitrate, and vice versa. The ultra-low bitrate compression can be achieved by adjusting the parameter λ .

3.2. Multi-stage Semantic Image Decoder

We have developed a multi-stage semantic image decoder that utilizes pre-trained controllable text-to-image diffusion models. This decoder restores adequate details in the image constrained by the extremely compressed reference image, text descriptions and semantic masks. This decoding process is implemented object-by-object progressively starting from the low-quality reference image, ultimately generating high-quality reconstructions that are highly consistent with the original images. In each decoding stage, we choose ControlNet as the decoder, a text-to-image model built on top of Stable Diffusion that can process spatial conditions in the form of the reference image. It ensures that the reconstructed images follow constraints provided by the essential structure of the input reference image, and text descriptions. In addition, we follow the pipeline similar to Mulan [22] to ensure that the generated object detail information is accurately positioned within the mask region given the object description $Text_d_j$ and the corresponding mask M_j . The complete procedure is listed in Algorithm 1 and described as follows.

Condition Encoding. In each stage, we utilize the fixed VAE encoder $\varepsilon(\bullet)$ to encode the reconstructed refer-

ence image I_j into the latent space for condition encoding: $cf_j = \varepsilon(I_j)$. In addition, CLIP text encoder, a pretrained model that provides a shared text-image embedding space, is utilized to produce the textual representations and inject them into the cross attention layers of the denoising U-Net.

Single-Object Restoration with Attention Guidance

Given the semantic mask M_j of object j and the reference image I_j , the next is to ensure the generated object details will be correctly located within M_j . A natural and intuitive approach to achieving this in diffusion models is to guide the generation of the cross-attention map for objects, thereby establishing correlations between text prompts and object locations. To this end, our method manipulates the cross-attention map under the guidance of the mask, employing a reverse guidance method to maximize the relevance within the mask region. Specifically, let $A_{m,k}$ denotes the cross-attention map which associates each spatial location m of the immediate feature in the denoising network to token k that describes object j in the prompt $Text_d_j$. Larger values in $A_{m,k}$ indicate a higher likelihood that the description is situated at that spatial location. The attention map is biased by introducing an energy function

$$E(\mathbf{A}, \mathbf{M}_j, k) = \left(1 - \frac{\sum_{m \in M_j} \mathbf{A}_{m,k}}{\sum_m \mathbf{A}_{m,k}}\right)^2 \quad (2)$$

where $\sum_{m \in M_j}$ denotes the summation over the spatial locations included in M_j , and \sum_m denotes the summation over all the spatial locations in the attention map. This energy function is optimized to maximize the correlation $A_{m,d}$ within the mask while minimizing the correlation outside of it. Specifically, at each application of ControlNet for image restoration, the gradient of the loss (2) is computed via backpropagation to update the latent $z_{j,t}$

$$z_{j,t} = z_{j,t} - \eta \cdot \nabla_{z_{j,t}} E(\mathbf{A}, \mathbf{M}_j, k) \quad (3)$$

where $\eta > 0$ is a scale factor controlling the strength of the guidance.

Meanwhile, to account for the preceding objects and their constraints during the restoration of the current object, we further combine the latent values of $z_{j,(t-1)}$ and $z_{(j-1),(t-1)}$. Specifically, following the step t in the reverse process (where t transitions from its initial value to 0), we update the latent variable $z_{j,(t-1)}$ as follows:

$$z_{j,(t-1)} = M_j \odot z_{j,t} + (1 - M_j) \odot z_{(j-1),(t-1)} \quad (4)$$

where \odot computes element-wise product.

After J iterations, we have successfully restored the detailed information for J objects in the reference image. Finally, we use the description text of the entire image, $Text_{all}$, to further restore the whole image. This step plays a crucial role in the decoding process as it ensures consistency and enhances perception scores of the entire image.

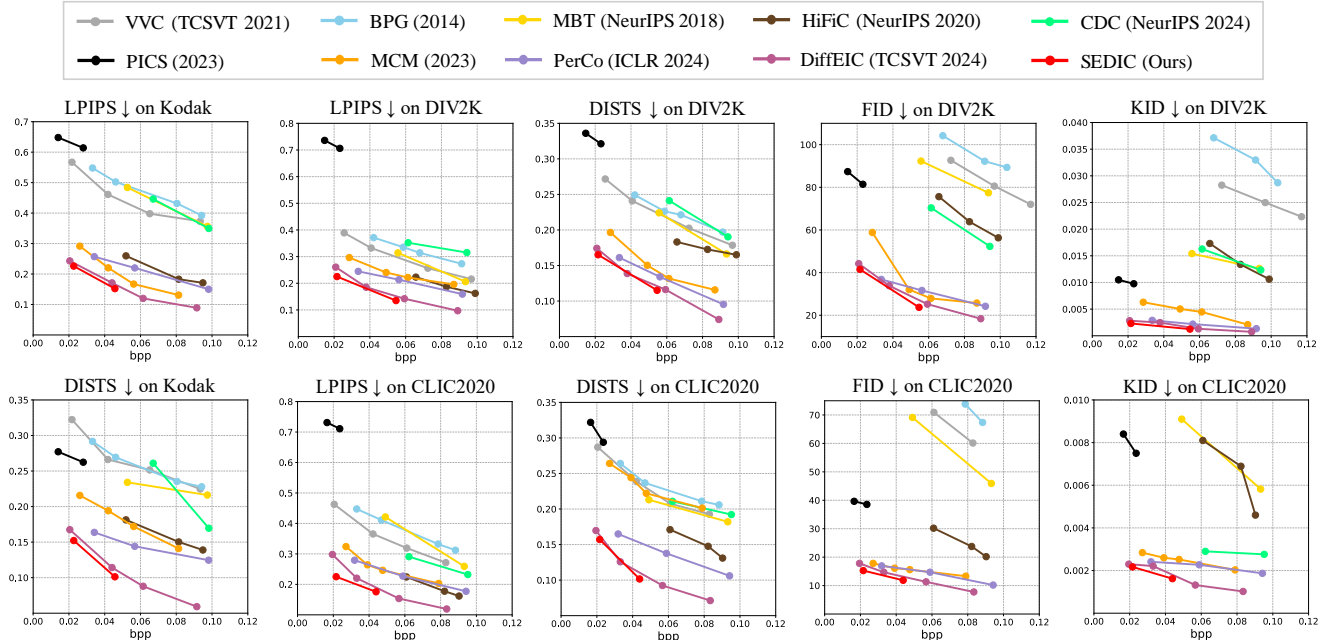


Figure 3. Quantitative comparisons with state-of-the-art methods in terms of perceptual quality (LPIPS↓ / DISTSt↓ / FID↓ / KID↓) on the Kodak [38], DIV2K validation [2], and CLIC2020 [41] datasets.

4. Experiments

4.1. Experimental Settings

Implementation: In our method, we keep the Image Textualization and Semantic Mask Encoder, along with diffusion models at the decoder (using default parameters from GPT-4 Vision [1], SAM [18], GroundingDino [26] and ControlNet [47]), frozen, focusing instead on fine-tuning an ultra-low bitrate image encoder/decoder based on the cheng2020-attn model from the deep image compression platform CompressAI [6]. Specifically, this process starts the model in its lowest bitrate mode, then increases the bitrate weight of the loss function tenfold (by reducing λ to 1/10 of its original value), thereby enabling extreme compression training with a learning rate of 10^{-4} . Our method, SEDIC, dynamically adjusts bitrates by tuning the number of objects J , text description length l_d and l_{all} . When the bitrate falls within the range of 0.02 to 0.03 bpp, J is set to 1, with l_d and l_{all} are designate as 20 and 30 words, respectively. When the bitrate is 0.04 ~ 0.05 bpp, J increases to 3, with l_d and l_{all} are designated as 30 and 50 words, respectively. This relatively high bitrate allows for more image details and thus better recovery. All experiments are conducted on a single NVIDIA GeForce RTX 4090 GPU.

Test Data: For evaluation, we utilize three commonly used benchmark datasets: Kodak [38], DIV2K validation [2], and CLIC2020 [41] datasets. The Kodak dataset consists of 24 natural images at a resolution of 768×512. The DIV2K validation dataset includes 100 super-resolution images, while the CLIC2020 dataset contains 428 high-quality images.

For the DIV2K validation and CLIC2020 datasets, we re-size images such that the shorter dimension is set to 768px. Subsequently, we center-crop each image to a resolution of 768×768 for evaluation purposes [44].

Metrics: We adopt a comprehensive set of compression evaluation metrics to address both consistency and perceptual quality requirements. Since semantic metrics become crucial at ultra-low bitrates, which better characterize the difference between compressed images and ground truth. They are prioritized over pixel-level metrics such as PSNR and SSIM. Specifically, we employ Learned Perceptual Image Patch Similarity (LPIPS) [48], a widely used visual metric based on the Human Visual System (HVS), and the Deep Image Structure and Texture Similarity (DISTSt) [12] metric to quantify compression-induced distortions. For perceptual evaluation, we use Frechet Inception Distance (FID) [16] and Kernel Inception Distance (KID) [9]. Additionally, the compression bitrate is assessed in terms of bits per pixel (bpp).

4.2. Experiment Results and Discussion

We compare our SEDIC with state-of-the-art image compression methods, including traditional compression standards VVC [10], BPG [7]; learned image compression approach MBT [30], GAN based HiFiC [28], Diffusion based approaches including CDC [44], PerCo [11], DiffeIC [23], Mask image modeling based MCM [20] and Text-to-Image model based PICS [19]. For VVC, we utilize the reference software VTM23.03 configured with intra-frame settings.

Quantitative Comparisons: Figure 3 presents the rate-



Figure 4. We visually compare the proposed SEDIC framework with stable diffusion-based methods, including PICS, PerCo, and DiffEIC on the Kodak and DIV2K validation datasets under ultra-low bitrate settings. We also include HiFiC at 0.1 \sim 0.2 bpp and the Ground Truth as references. For each method, the corresponding bpp and LPIPS values are displayed below the images. Compared to other approaches, our method produces more realistic and faithful reconstructions while achieving lower bpp.

distortion-perception curves of various methods on three datasets under ultra-low bitrate settings. It can be observed that our proposed SEDIC consistently outperforms state-of-the-art (SOTA) image compression approaches across all distortion and perception metrics, showing better semantic consistency and perceptual performance. BPG [7], VVC [40] and MBT[30] optimize the rate-distortion function in terms of mean square error, leading to poor perception quality in terms of FID, DISTS and LPIPS. By contrast, Generative image compression approaches exhibits much better perception quality even at low bitrates, including HiFiC [28] PerCo [11] and DiffEIC [23], PICS [19] and etc. Among these generative approaches, PICS [19] encodes images into simple text and rough sketches, results in poor semantic consistency (high LPIPS and DISTS) despite of high perception quality (low FID). DiffEIC [23] becomes the SOTA baseline in terms of perception quality and semantic consistency. Compared with DiffEIC, our proposed SEDIC method still outperforms DiffEIC [24] with a great margin.

Qualitative Comparisons: Figure 4 presents a visual comparison of evaluated methods under extremely low bitrates. We visualize the performance of stable diffusion-based methods PICS, PerCo, DiffEIC and our proposed SEDIC at ultra-low bitrates, along with HiFiC results at a 0.1 \sim

0.2 bpp setting as a reference. Compared to other methods, SEDIC achieves reconstructions with higher perceptual quality, fewer artifacts, and more realistic details at extremely low bitrates. For example, SEDIC preserves the fine details of the tower’s peak that are lost or distorted in other methods (see the first row). Similarly, SEDIC generates more realistic fur details (e.g., the squirrel’s tail in the second row). Additionally, SEDIC better retains background cloud details (see the third row). Remarkably, our method achieves visually comparable performance to HiFiC at only one-tenth of HiFiC’s bpp, demonstrating even better perceptual quality. More qualitative comparison results can be found in the supplementary material.

4.3. Ablation Study

We conducted an ablation study to evaluate the contribution of different semantically encoding components within SEDIC, as shown in Table 1. These components are designated as: 1) number of objects, 2) Overall Description of the image $Text_{all}$, 3) extremely compressed reference image \tilde{I}_0 , and 4) object description length l_d and overall description length l_{all} . The results indicate that the extremely compressed reference image is the most essential component. Absence of the extremely compressed reference image brings dramatic perception quality degradation (Line 6 vs 7). Furthermore, the perception quality is incrementally



Figure 5. Visual comparisons of different denoising steps. 0 step denotes the reference image as the starting point.

| Serial No. | Content | | | | | (LPIPS ↓ ,bpp) | (DISTIS ↓ ,bpp) |
|------------|---------|--------------|---------------|-------------|-----------------|------------------|------------------|
| | J | $Text_{all}$ | \tilde{I}_0 | l_d words | l_{all} words | | |
| 1 | 0 | ✓ | ✓ | | 50 | (0.2338, 0.0226) | (0.1667, 0.0226) |
| 2 | 1 | ✓ | ✓ | 30 | 50 | (0.2260, 0.0304) | (0.1522, 0.0304) |
| 3 | 1 | | ✓ | 30 | | (0.2517, 0.0258) | (0.1760, 0.0258) |
| 4 | 2 | | ✓ | 30 | | (0.2327, 0.0334) | (0.1641, 0.0334) |
| 5 | 3 | | ✓ | 30 | | (0.2243, 0.0412) | (0.1503, 0.0412) |
| 6 | 3 | ✓ | ✓ | 30 | 50 | (0.1518, 0.0457) | (0.1012, 0.0457) |
| 7 | 3 | ✓ | ✓ | 30 | 50 | (0.3518, 0.0275) | (0.2284, 0.0275) |
| 8 | 3 | ✓ | ✓ | 10 | 50 | (0.1718, 0.0413) | (0.1318, 0.0413) |
| 9 | 3 | ✓ | ✓ | 30 | 30 | (0.1651, 0.0442) | (0.1151, 0.0442) |

Table 1. Ablation validation on Kodak [38] dataset. J represent the number of objects, $Text_{all}$ represent the Overall Image Description, \tilde{I}_0 represent the reference image, l_d words denote the length of the object details, and l_{all} words represent the length of the Overall Image Description.

| Method | Denoising Step | Encoding Speed(in sec.) | Decoding Speed(in sec.) | Platform |
|-------------|----------------|-------------------------|-------------------------|---------------------|
| VVC | - | 13.862 ± 9.821 | 0.066 ± 0.006 | 13th Core i9-13900K |
| HfFiC | - | 0.038 ± 0.004 | 0.059 ± 0.004 | RTX4090 |
| PICS | 25 | 62.045 ± 0.516 | 12.028 ± 0.413 | RTX4090 |
| PerCo | 20 | 0.080 ± 0.018 | 2.551 ± 0.018 | A100 |
| DiffEIC | 20 | 0.128 ± 0.005 | 1.964 ± 0.009 | RTX4090 |
| DiffEIC | 50 | 0.128 ± 0.005 | 4.574 ± 0.006 | RTX4090 |
| SEDIC(Ours) | 20 | 0.157 ± 0.013 | 2.332 ± 0.003 | RTX4090 |
| SEDIC(Ours) | 50 | 0.157 ± 0.013 | 4.994 ± 0.003 | RTX4090 |

Table 2. Encoding and decoding speed (in seconds) on Kodak [38].

improved by increasing the number of objects to restore the object-level semantic details upon the reference image, demonstrating the effectiveness of our object-level semantic compression (from Line3 to 5). Additionally, the Overall Description also brings overall perception quality improvement during the decoding process. The word lengths of object descriptions l_d and overall descriptions l_{all} have a slight impact on the results (Line3 vs 2). In summary, all of the encoding components in our proposed SEDIC make contributions to the ultimately satisfying perception performance.

4.4. Effect of Denoising Steps

Figure 6 illustrates the reconstruction performance using varying numbers of denoising steps. We observe that increasing the number of denoising steps enhances the perceptual quality of the decoded results. However, with an extremely low number of steps (e.g., 5 steps), the reconstructed image quality is significantly degraded. Additionally, when the number of denoising steps exceeds 30, the reconstruction quality tends to stabilize. The visual results in Figure 5 further demonstrates that more realistic and refined details will be restored as the denoising steps increase.

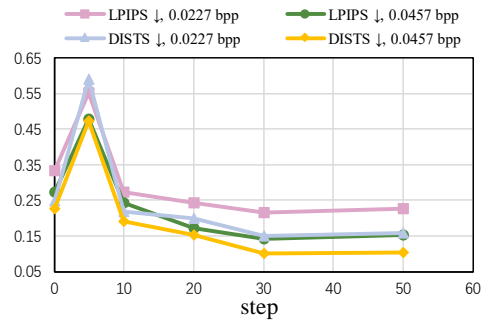


Figure 6. Quantitative comparisons of different denoising steps on Kodak [38]. 0 step denotes directly using reference image.

4.5. Complexity Analysis

We further compare the proposed SEDIC with SOTA image compression methods in terms of computational complexity. For PerCo [11], we report the results as stated in their paper, as the official source code is unavailable. Table 2 summarizes the average encoding/decoding time on the Kodak dataset (in seconds), along with standard deviations. Notably, diffusion based methods have higher encoding and decoding complexity compared to VAE and GAN based approaches. In addition, PICS[19] needs to perform projection gradient search in the CLIP embedding space to generate text, which takes a significant amount of time. the proposed SEDIC encoder is significantly faster than PICS. Compared to other methods PerCo and DiffEIC based on pretrained diffusion models, SEDIC achieves comparable encoding and faster decoding speeds with the same number of denoising steps.

5. Conclusion

We propose a novel image compression framework, named SEDIC, which leverage LMMs to achieve ultra-low bitrate compression while maintaining high semantic consistency and perceptual quality. Specifically, the SEDIC approach leverages LMMs to decompose the images into compact semantic representations, including an extremely compressed reference image, overall and object-level text descriptions and the semantic masks. The multi-stage decoder employs controllable diffusion models to restore high-quality, semantically consistent images object-by-object progressively starting from the reference image. Experimental results demonstrate that SEDIC significantly outperforms

SOTA image compression methods in terms of perceptual quality at ultra-low bitrates (≤ 0.05 bpp). We believe that this LMMs driven approach has the potential to pave the way for a new paradigm in image compression.

References

- [1] Josh Achiam, Steven Adler, Sandhini Agarwal, Lama Ahmad, Ilge Akkaya, Florencia Leoni Aleman, Diogo Almeida, Janko Altenschmidt, Sam Altman, Shyamal Anadkat, et al. Gpt-4 technical report. *arXiv preprint arXiv:2303.08774*, 2023. 2, 4, 6
- [2] Eirikur Agustsson and Radu Timofte. Ntire 2017 challenge on single image super-resolution: Dataset and study. In *Proceedings of the IEEE conference on computer vision and pattern recognition workshops*, pages 126–135, 2017. 6
- [3] Omri Avrahami, Thomas Hayes, Oran Gafni, Sonal Gupta, Yaniv Taigman, Devi Parikh, Dani Lischinski, Ohad Fried, and Xi Yin. Spatext: Spatio-textual representation for controllable image generation. In *Proceedings of the IEEE/CVF Conference on Computer Vision and Pattern Recognition*, pages 18370–18380, 2023. 3
- [4] Johannes Ballé, Valero Laparra, and Eero P Simoncelli. End-to-end optimized image compression. *arXiv preprint arXiv:1611.01704*, 2016. 1
- [5] Johannes Ballé, David Minnen, Saurabh Singh, Sung Jin Hwang, and Nick Johnston. Variational image compression with a scale hyperprior. *arXiv preprint arXiv:1802.01436*, 2018. 1
- [6] Jean Bégaint, Fabien Racapé, Simon Feltman, and Akshay Pushparaja. Compressai: a pytorch library and evaluation platform for end-to-end compression research. *arXiv preprint arXiv:2011.03029*, 2020. 4, 6
- [7] Fabrice Bellard. Bpg image format. [Online]. <https://bellard.org/bpg/>. 6, 7
- [8] Shariq Farooq Bhat, Niloy Mitra, and Peter Wonka. Loosecontrol: Lifting controlnet for generalized depth conditioning. In *ACM SIGGRAPH 2024 Conference Papers*, pages 1–11, 2024. 3
- [9] Mikołaj Bińkowski, Danica J Sutherland, Michael Arbel, and Arthur Gretton. Demystifying mmd gans. *arXiv preprint arXiv:1801.01401*, 2018. 6
- [10] Benjamin Bross, Ye-Kui Wang, Yan Ye, Shan Liu, Jianle Chen, Gary J Sullivan, and Jens-Rainer Ohm. Overview of the versatile video coding (vvc) standard and its applications. *IEEE Transactions on Circuits and Systems for Video Technology*, 31(10):3736–3764, 2021. 6
- [11] Marlene Careil, Matthew J Muckley, Jakob Verbeek, and Stéphane Lathuilière. Towards image compression with perfect realism at ultra-low bitrates. In *The Twelfth International Conference on Learning Representations*, 2023. 6, 7, 8
- [12] Keyan Ding, Kede Ma, Shiqi Wang, and Eero P Simoncelli. Image quality assessment: Unifying structure and texture similarity. *IEEE transactions on pattern analysis and machine intelligence*, 44(5):2567–2581, 2020. 6
- [13] Junlong Gao, Chuanmin Jia, Zhimeng Huang, Shanshe Wang, Siwei Ma, and Wen Gao. Rate-distortion optimized cross modal compression with multiple domains. *IEEE Transactions on Circuits and Systems for Video Technology*, 2024. 4
- [14] Songwei Ge, Taesung Park, Jun-Yan Zhu, and Jia-Bin Huang. Expressive text-to-image generation with rich text. In *Proceedings of the IEEE/CVF International Conference on Computer Vision*, pages 7545–7556, 2023. 2
- [15] Solomon Golomb. Run-length encodings (corresp.). *IEEE transactions on information theory*, 12(3):399–401, 1966. 4
- [16] Martin Heusel, Hubert Ramsauer, Thomas Unterthiner, Bernhard Nessler, and Sepp Hochreiter. Gans trained by a two time-scale update rule converge to a local nash equilibrium. *Advances in neural information processing systems*, 30, 2017. 6
- [17] Wenyi Hong, Weihang Wang, Qingsong Lv, Jiazheng Xu, Wenmeng Yu, Junhui Ji, Yan Wang, Zihan Wang, Yuxiao Dong, Ming Ding, et al. Cogagent: A visual language model for gui agents. In *Proceedings of the IEEE/CVF Conference on Computer Vision and Pattern Recognition*, pages 14281–14290, 2024. 2
- [18] Alexander Kirillov, Eric Mintun, Nikhila Ravi, Hanzi Mao, Chloe Rolland, Laura Gustafson, Tete Xiao, Spencer Whitehead, Alexander C Berg, Wan-Yen Lo, et al. Segment anything. In *Proceedings of the IEEE/CVF International Conference on Computer Vision*, pages 4015–4026, 2023. 2, 4, 6
- [19] Eric Lei, Yiğit Berkay Uslu, Hamed Hassani, and Shirin Saeedi Bidokhti. Text+ sketch: Image compression at ultra low rates. *arXiv preprint arXiv:2307.01944*, 2023. 2, 3, 4, 6, 7, 8
- [20] Anqi Li, Feng Li, Jiabin Han, Huihui Bai, Runmin Cong, Chunjie Zhang, Meng Wang, Weisi Lin, and Yao Zhao. You can mask more for extremely low-bitrate image compression. *arXiv preprint arXiv:2306.15561*, 2023. 6
- [21] Chunyi Li, Haoyang Li, Ning Yang, and Dazhi He. A pbch reception algorithm in 5g broadcasting. In *2022 IEEE International Symposium on Broadband Multimedia Systems and Broadcasting (BMSB)*, pages 1–6. IEEE, 2022. 1
- [22] Sen Li, Ruochen Wang, Cho-Jui Hsieh, and Minhao Cheng. Mulan: Multimodal-llm agent for progressive and interactive multi-object diffusion. *arXiv preprint arXiv:2402.12741*, 2024. 3, 5
- [23] Zhiyuan Li, Yanhui Zhou, Hao Wei, Chenyang Ge, and Jingwen Jiang. Towards extreme image compression with latent feature guidance and diffusion prior. *arXiv preprint arXiv:2404.18820*, 2024. 6, 7
- [24] Xinqi Lin, Jingwen He, Ziyang Chen, Zhaoyang Lyu, Bo Dai, Fanghua Yu, Wanli Ouyang, Yu Qiao, and Chao Dong. Diffbir: Towards blind image restoration with generative diffusion prior. *arXiv preprint arXiv:2308.15070*, 2023. 3, 7
- [25] Haotian Liu, Chunyuan Li, Qingyang Wu, and Yong Jae Lee. Visual instruction tuning. *Advances in neural information processing systems*, 36, 2024. 2
- [26] Shilong Liu, Zhaoyang Zeng, Tianhe Ren, Feng Li, Hao Zhang, Jie Yang, Chunyuan Li, Jianwei Yang, Hang Su, Jun Zhu, et al. Grounding dino: Marrying dino with grounded pre-training for open-set object detection. *arXiv preprint arXiv:2303.05499*, 2023. 2, 4, 6

- [27] Yuliang Liu, Biao Yang, Qiang Liu, Zhang Li, Zhiyin Ma, Shuo Zhang, and Xiang Bai. Textmonkey: An ocr-free large multimodal model for understanding document. *arXiv preprint arXiv:2403.04473*, 2024. 2
- [28] Fabian Mentzer, George D Toderici, Michael Tschannen, and Eirikur Agustsson. High-fidelity generative image compression. *Advances in Neural Information Processing Systems*, 33:11913–11924, 2020. 2, 6, 7
- [29] David Minnen and Saurabh Singh. Channel-wise autoregressive entropy models for learned image compression. In *2020 IEEE International Conference on Image Processing (ICIP)*, pages 3339–3343. IEEE, 2020. 1
- [30] David Minnen, Johannes Ballé, and George D Toderici. Joint autoregressive and hierarchical priors for learned image compression. *Advances in neural information processing systems*, 31, 2018. 6, 7
- [31] David Minnen, Johannes Ballé, and George D Toderici. Joint autoregressive and hierarchical priors for learned image compression. *Advances in neural information processing systems*, 31, 2018. 1
- [32] Matthew J Muckley, Alaaeldin El-Nouby, Karen Ullrich, Hervé Jégou, and Jakob Verbeek. Improving statistical fidelity for neural image compression with implicit local likelihood models. In *International Conference on Machine Learning*, pages 25426–25443. PMLR, 2023. 2
- [33] Fumitaka Ono, William Rucklidge, Ronald Arps, and Corneliu Constantinescu. Jbig2-the ultimate bi-level image coding standard. In *Proceedings 2000 international conference on image processing (Cat. No. 00CH37101)*, pages 140–143. IEEE, 2000. 4
- [34] Zhihong Pan, Xin Zhou, and Hao Tian. Extreme generative image compression by learning text embedding from diffusion models. *arXiv preprint arXiv:2211.07793*, 2022. 2, 3
- [35] Renjie Pi, Jianshu Zhang, Jipeng Zhang, Rui Pan, Zhekai Chen, and Tong Zhang. Image textualization: An automatic framework for creating accurate and detailed image descriptions. *arXiv preprint arXiv:2406.07502*, 2024. 3
- [36] Alec Radford, Jong Wook Kim, Chris Hallacy, Aditya Ramesh, Gabriel Goh, Sandhini Agarwal, Girish Sastry, Amanda Askell, Pamela Mishkin, Jack Clark, et al. Learning transferable visual models from natural language supervision. In *International conference on machine learning*, pages 8748–8763. PMLR, 2021. 2
- [37] Aditya Ramesh, Prafulla Dhariwal, Alex Nichol, Casey Chu, and Mark Chen. Hierarchical text-conditional image generation with clip latents. *arXiv preprint arXiv:2204.06125*, 1(2):3, 2022. 2
- [38] Rich Franzen. Kodak lossless true color image suite, 2012. <https://bellard.org/bpg/>. 6, 8
- [39] Robin Rombach, Andreas Blattmann, Dominik Lorenz, Patrick Esser, and Björn Ommer. High-resolution image synthesis with latent diffusion models. In *Proceedings of the IEEE/CVF conference on computer vision and pattern recognition*, pages 10684–10695, 2022. 2
- [40] Joint Video Experts Team. Vvc official test model vtm. <https://jvet.hhi.fraunhofer.de/>, 2021. 1, 7
- [41] George Toderici, Lucas Theis, Nick Johnston, Eirikur Agustsson, Fabian Mentzer, Johannes Ballé, Wenzhe Shi, and Radu Timofte. Clic 2020: Challenge on learned image compression, 2020, 2020. 6
- [42] Hugo Touvron, Thibaut Lavril, Gautier Izacard, Xavier Martinet, Marie-Anne Lachaux, Timothée Lacroix, Baptiste Rozière, Naman Goyal, Eric Hambro, Faisal Azhar, et al. Llama: Open and efficient foundation language models. *arXiv preprint arXiv:2302.13971*, 2023. 2
- [43] Gregory K Wallace. The jpeg still picture compression standard. *IEEE transactions on consumer electronics*, 38(1): xviii–xxxiv, 1992. 1
- [44] Ruihan Yang and Stephan Mandt. Lossy image compression with conditional diffusion models. *Advances in Neural Information Processing Systems*, 36, 2024. 2, 6
- [45] Haoxuan You, Haotian Zhang, Zhe Gan, Xianzhi Du, Bowen Zhang, Zirui Wang, Liangliang Cao, Shih-Fu Chang, and Yinfei Yang. Ferret: Refer and ground anything anywhere at any granularity. *arXiv preprint arXiv:2310.07704*, 2023. 2
- [46] Lvmin Zhang, Anyi Rao, and Maneesh Agrawala. Adding conditional control to text-to-image diffusion models. In *Proceedings of the IEEE/CVF International Conference on Computer Vision*, pages 3836–3847, 2023. 2
- [47] Lvmin Zhang, Anyi Rao, and Maneesh Agrawala. Adding conditional control to text-to-image diffusion models. In *Proceedings of the IEEE/CVF International Conference on Computer Vision*, pages 3836–3847, 2023. 3, 6
- [48] Richard Zhang, Phillip Isola, Alexei A Efros, Eli Shechtman, and Oliver Wang. The unreasonable effectiveness of deep features as a perceptual metric. In *Proceedings of the IEEE conference on computer vision and pattern recognition*, pages 586–595, 2018. 6
- [49] Zicheng Zhang, Yingjie Zhou, Long Teng, Wei Sun, Chunyi Li, Xiongkuo Min, Xiao-Ping Zhang, and Guangtao Zhai. Quality-of-experience evaluation for digital twins in 6g network environments. *IEEE Transactions on Broadcasting*, 2024. 1